

Control Assembly and Reversible Transformation of Tuneable

Luminescent Mo₈-R6G Hybrids

Hui-Min Zeng, Wei-Hong Wu, Chao Wang, Zhan-Guo Jiang*, Cai-Hong Zhan*

Table of Contents

S1	Materials
S2	General Experimental Section
	Powder X-ray Diffraction (PXRD)
	Fourier Transform Infrared Spectroscopy (FTIR)
	Thermogravimetric Analyses (TGA)
	Elemental Analyses (EA)
	UV-Vis absorption spectra (UV)
	Fluorescence emission and excitation spectra
	Fluorescence quantum yield
	Luminescence decay measurements
	Single-crystal X-ray diffraction (SCXRD)
S3	Synthesis and Experimental Section
	Synthesis of Mo₈-(R6G)₂
	Synthesis of Mo₈-(R6G)₄
S4	Crystal data and structure refinement
S5	Fourier Transform Infrared Spectroscopy (FTIR)
S6	Powder X-ray diffraction (PXRD)
S7	Thermogravimetric analyses (TGA)
S8	UV-Vis absorption spectra
S9	The band gap
S11	The Excitation spectroscopy of solid-state samples
S11	The Steady state photoluminescence (PL) spectroscopy of solid-state samples
S12	Emission decay spectroscopy
S13	The fluorescence emission spectra of CH₃CN solution
S14	Reference

S1 Materials

All the chemicals, whether reagents or solvent, were purchased from suppliers and used as received without further purification. Molybdenum trioxide (MoO_3 , 99.5%) Tetrabutylammonium hydroxide ($[(n\text{-C}_4\text{H}_9)_4\text{N}]\text{OH}$, 25 % aqueous solution), and Rhodamine 6G chloride ($\text{C}_{28}\text{H}_{31}\text{ClN}_2\text{O}_3$, R6G) were purchased from Aladdin. acetonitrile (CH_3CN , AR) was purchased from Sinopharm Chemical Reagent Co., Ltd., China.

S2 General Experimental Section

Powder X-ray Diffraction (PXRD)

Powder XRD patterns were recorded on a Bruker D8 Advance X-ray diffractometer with (λ ($\text{CuK}\alpha$) = 1.5405 Å) radiation in the 2θ range of 4-50°.

Fourier Transform Infrared Spectroscopy (FTIR)

FTIR Spectroscopy (KBr pellets) were obtained from a Nicolet NEXUS 670 spectrometer in the range of 400 and 4000 cm^{-1} .

Thermogravimetric Analyses (TGA)

Thermogravimetric Analyses were carried out under N_2 atmosphere on a TA Instruments STA499 F5 thermobalance at the rate of 10 °C/min heating from 20 °C to 800 °C.

Elemental Analyses (EA)

H microanalyse was performed on a Perkin-Elmer 240C elemental analyser, and ICP-OES analyses were carried out on a PerkinElmer Optima 8300 optical emission spectrometer.

UV-Vis absorption spectra (UV)

Solid state UV-Vis absorption spectra were acquired on a Carry 5000 spectrophotometer, in which the range of wavenumber was setted at 200 to 800 nm. The UV-vis spectra in CH_3CN solution were recorded on an UV5500PC

spectrophotometer from 200 to 800 nm using 1.000-cm-optical-path quartz cuvettes.

Fluorescence emission and excitation spectra

The Steady-state photoluminescence (PL) spectroscopy for the solid-state samples (the fluorescence emission spectra is recorded with various excitation wavelength in the range of 310 to 590 nm) were obtained on the FLS 980 spectrometer.

The excitation spectra of the three solid samples were recorded on the FLS980 spectrometer with the maximum emission wavelength 660 nm.

Luminescence decay measurements

Time-resolved emission spectroscopy (TRES) were performed on a FLS980 spectrofluorometer and recorded using the time-correlated single-photon counting (TCSPC) method. (excitation wavelength, 570 nm; emission wavelength, 629nm, slit, 5 nm).

Single-crystal X-ray diffraction (SCXRD)

Single-crystal X-ray diffraction data collection of $\text{Mo}_8\text{-(R6G)}_2$ and $\text{Mo}_8\text{-(R6G)}_4$ were recorded on Bruker D8 VENTURE diffractometer equipped with a PHOTON 100 CMOS bidimensional detector and MoK α monochromatized radiation ($\lambda = 0.71073 \text{ \AA}$) at 150 K. The structure of target compounds were solved by intrinsic phasing methods and refined by full-matrix least squares using the SHELX-TL package¹. All of the non-hydrogen atoms are dealt with anisotropic thermal parameters. Hydrogen atoms on water are not identified. Further details about of the crystal structure determinations may be obtained free of charge via the Internet at <https://www.ccdc.cam.ac.uk/> CCDC 2090079, 2090082. Crystallographic data for single-crystal X-ray diffraction studies are summarized in Table S1.

S3 Synthesis and Experimental Section

Synthesis of $[\text{N}(\text{C}_4\text{H}_9)_4]_4[\alpha\text{-Mo}_8\text{O}_{26}]$

Molybdenum(VI) oxide (MoO_3 , 1.2 g, 8.3 mmol) was mixed with aqueous $[(n\text{-C}_4\text{H}_9)_4\text{N}]\text{OH}$ (10 mL, 4.1 mmol). The mixture was stirred for 60 h, during which time the pH of the mixture went down from 7.8 to 6.1 and the slightly gray suspension turned bright white. The precipitate was collected on a fine-porosity filter with suction and dried in vacuo over P_2O_5 . This crude product (2.1 g) was dissolved in 15 mL of acetonitrile. After a small amount of insoluble material was filtered off with a fine-porosity filter, the filtrate was stored overnight at -4°C . The clear, colorless, block-

shaped crystals that formed were collected on a medium-porosity filter with suction and dried *in vacuo* over P_2O_5 for 8 h to yield 1.6 g of the product (0.74 mmol, 72%).

Synthesis of $Mo_8-(R6G)_2$

900 μ L of $(TBA)_4[Mo_8O_{26}]$ (0.1 g) dissolved into 10 mL of acetonitrile was added into Rhodamine 6G chloride (0.01 g) dissolved into 10 mL of acetonitrile. After 12 h, the clear yellow solution was filtered, and then allowed to evaporate in a Centrifuge tube at room temperature. The reddish brown rod crystal was obtained and collected by filtration and air-dried. Yield: 21.1 % based on Mo. FT-IR spectrum of **1** is given in Fig. S6. Elemental analysis: Calc. (found): H 5.2 (5.3); Mo 30.0 (32.1); C 41.3 (42.3); N 3.3 (3.0).

Synthesis of $Mo_8-(R6G)_4$

300 μ L of $(TBA)_4[Mo_8O_{26}]$ (0.1g) dissolved into 10 mL of acetonitrile was added into 2 mL of Rhodamine 6G chloride (0.01g) dissolved into 10 mL of acetonitrile. The clear yellow solution was allowed to evaporate in a Centrifuge tube at room temperature. After one day, reddish brown block crystal was obtained and collected by filtration and air-dried. Yield: 21.1 % based on Mo. FT-IR spectrum of **1** is given in Fig. S6. Elemental analysis: Calc. (found): H 4.2 (4.4); Mo 26.0 (26.8); C 45.4 (45.7); N 3.8 (3.6).

S4 Crystal data and structure refinement

Table S1. Crystal data and structure refinement for Mo₈-(R6G)₂ and Mo₈-(R6G)₄.

Empirical formula	C ₈₈ H ₁₃₄ Mo ₈ N ₆ O ₃₂	Empirical formula	C ₁₁₂ H ₁₂₄ Mo ₈ N ₈ O ₃₈
Formula weight	2555.52	Formula weight	2957.7
Temperature/K	273.15	Temperature/K	150
Crystal system	triclinic	Crystal system	triclinic
Space group	P-1	Space group	P-1
a/Å	13.4749(6)	a/Å	13.8480(6)
b/Å	14.2438(6)	b/Å	14.4144(7)
c/Å	15.6103(6)	c/Å	17.1863(8)
α/°	89.429(2)	α/°	99.426(2)
β/°	78.8110(10)	β/°	108.483(2)
γ/°	66.0940(10)	γ/°	96.850(2)
Volume/Å ³	2679.16(19)	Volume/Å ³	3155.5(3)
Z	1	Z	1
ρ _{calc} /cm ³	1.584	ρ _{calc} /cm ³	1.556
μ/mm ⁻¹	0.98	μ/mm ⁻¹	0.848
F(000)	1296	F(000)	1492
Crystal size/mm ³	0.3 × 0.2 × 0.1	Crystal size/mm ³	0.3 × 0.2 × 0.1
Radiation	MoKα (λ = 0.71073)	Radiation	MoKα (λ = 0.71073)
2θ range for data collection/°	4.704 to 54.994	2θ range for data collection/°	4.428 to 55.014
Index ranges	-17 ≤ h ≤ 17, -17 ≤ k ≤ 18, -20 ≤ l ≤ 18	Index ranges	-17 ≤ h ≤ 17, -18 ≤ k ≤ 18, -22 ≤ l ≤ 22
Reflections collected	31498	Reflections collected	51479
Independent reflections	12188 [R _{int} = 0.0276, R _{sigma} = 0.0375]	Independent reflections	14414 [R _{int} = 0.0273, R _{sigma} = 0.0257]
Data/restraints/parameters	12188/1/613	Data/restraints/parameters	14414/0/758
Goodness-of-fit on F ²	1.118	Goodness-of-fit on F ²	1.093
Final R indexes [I ≥ 2σ (I)]	R ₁ = 0.0432, wR ₂ = 0.1294	Final R indexes [I ≥ 2σ (I)]	R ₁ = 0.0515, wR ₂ = 0.1579
Final R indexes [all data]	R ₁ = 0.0560, wR ₂ = 0.1418	Final R indexes [all data]	R ₁ = 0.0590, wR ₂ = 0.1658

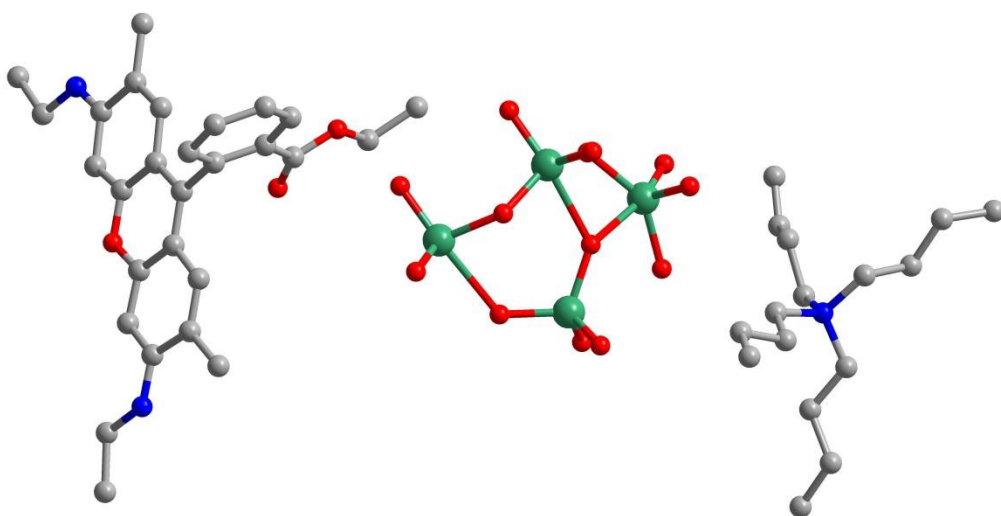


Fig. S1. Asymmetric unit of $\text{Mo}_8\text{-(R6G)}_2$.

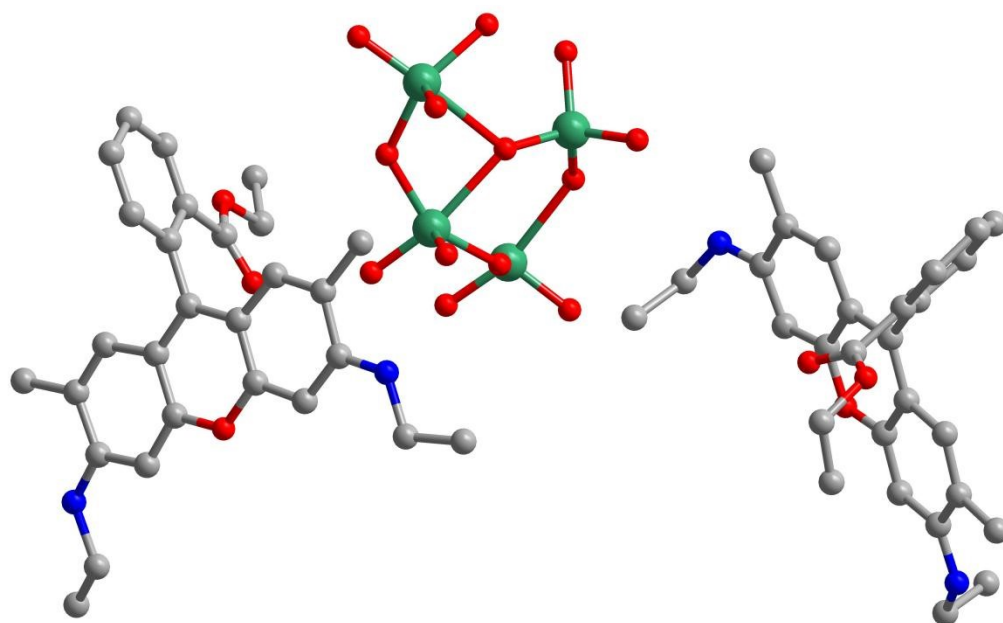


Fig. S2. Asymmetric unit of $\text{Mo}_8\text{-(R6G)}_4$.

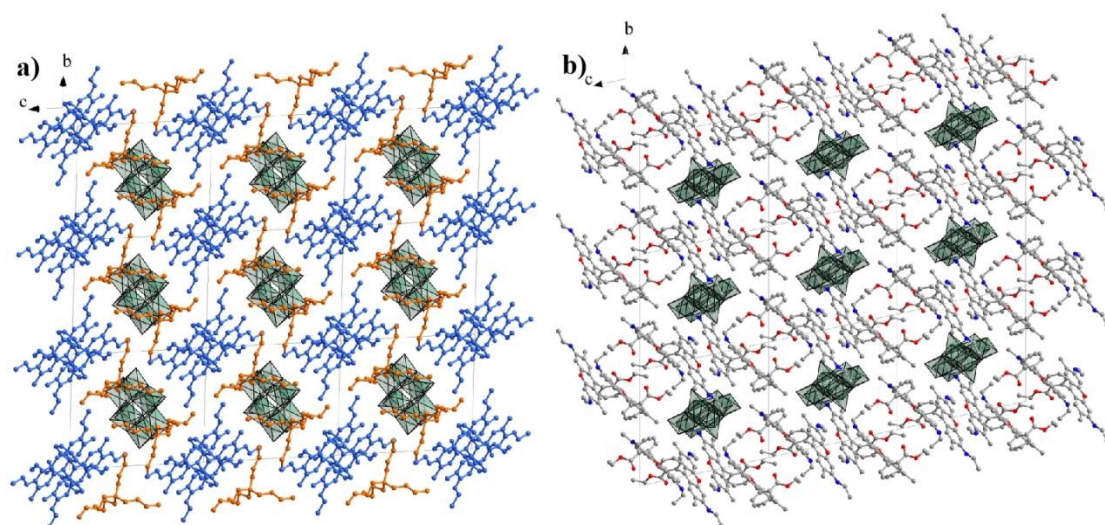


Fig. S3. Mixed polyhedral and ball-and-stick representations of the crystal packing in $\text{Mo}_8\text{-(R6G)}_2$ (a), $\text{Mo}_8\text{-(R6G)}_4$ (b) along the a axis.

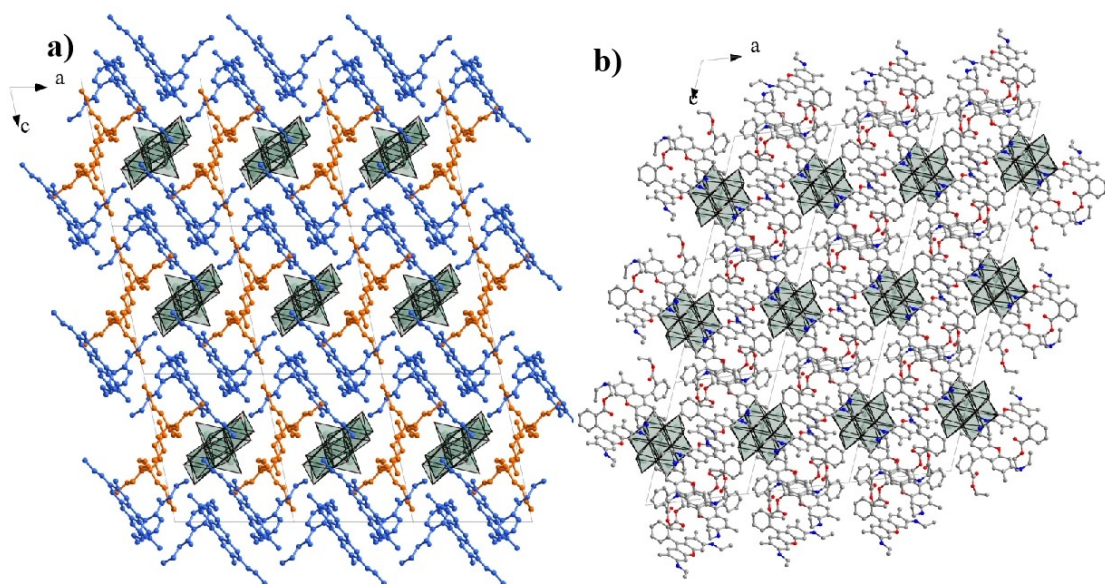


Fig. S4. Mixed polyhedral and ball-and-stick representations of the crystal packing in $\text{Mo}_8\text{-(R6G)}_2$ (a), $\text{Mo}_8\text{-(R6G)}_4$ (b) along the b axis.

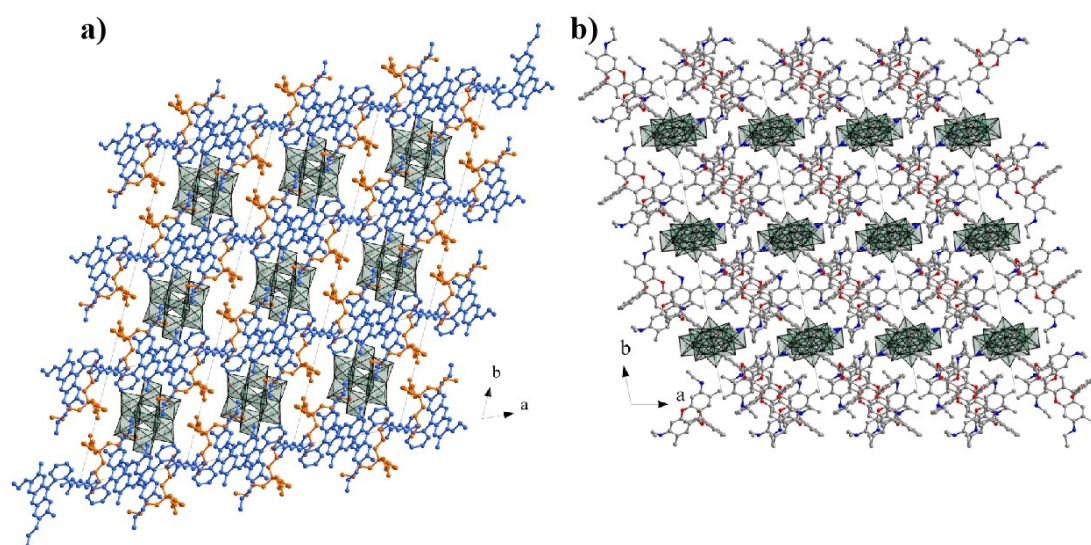


Fig. S5. Mixed polyhedral and ball-and-stick representations of the crystal packing in Mo₈-(R6G)₂ (a), Mo₈-(R6G)₄ (b) along the c axis.

S5 Fourier Transform Infrared

Spectroscopy (FTIR)

The IR spectrum of $\text{Mo}_8\text{-(R6G)}_2$ and $\text{Mo}_8\text{-(R6G)}_4$ are showed in the Fig. S6. The absorb band in the range of 1000 cm^{-1} to 400 cm^{-1} were attributed to the Mo=O and Mo-O-Mo vibration modes. Moreover, the absorb band of about 3000 cm^{-1} for $\text{Mo}_8\text{-(R6G)}_2$, R6G and $\text{Mo}_8\text{-(R6G)}_4$ were assigned to =CH stretching vibration of benzene ring. Besides, the absorb band of 3300 cm^{-1} belongs to C-H stretching vibration of methyl.

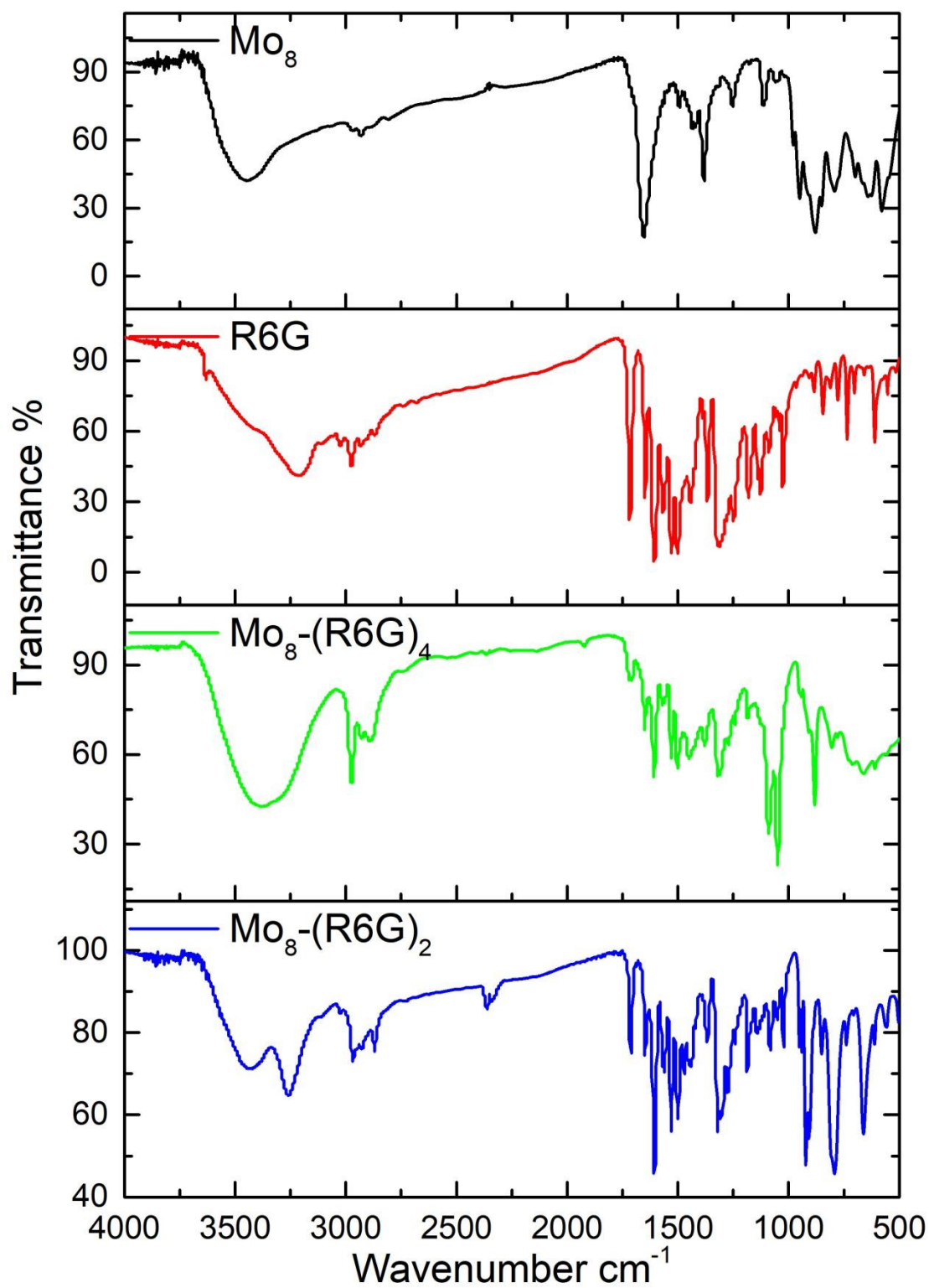


Fig. S6. FT-IR spectra of $\text{Mo}_8-(\text{R6G})_2$ (blue), $\text{Mo}_8-(\text{R6G})_4$ (green), R6G (red) and TBA- Mo_8 (black).

S6 Powder X-ray diffraction (PXRD)

The experimental and simulated PXRD patterns for $\text{Mo}_8\text{-(R6G)}_2$ and $\text{Mo}_8\text{-(R6G)}_4$ are shown in Figure S7-S8. Their powder X-ray diffraction (PXRD) patterns can be compared with the simulated pattern obtained from the X-ray single-crystal diffraction analysis. Their peak positions are in good agreement with each other, indicating the phase purity of the product. The differences in intensity may be due to the preferred orientation of the powder sample. Moreover, the peak positions of $\text{Mo}_8\text{-(R6G)}_2$ and $\text{Mo}_8\text{-(R6G)}_4$ are more than just the additional of TBA- Mo_8 and R6G. This may be due to the existence of interaction.

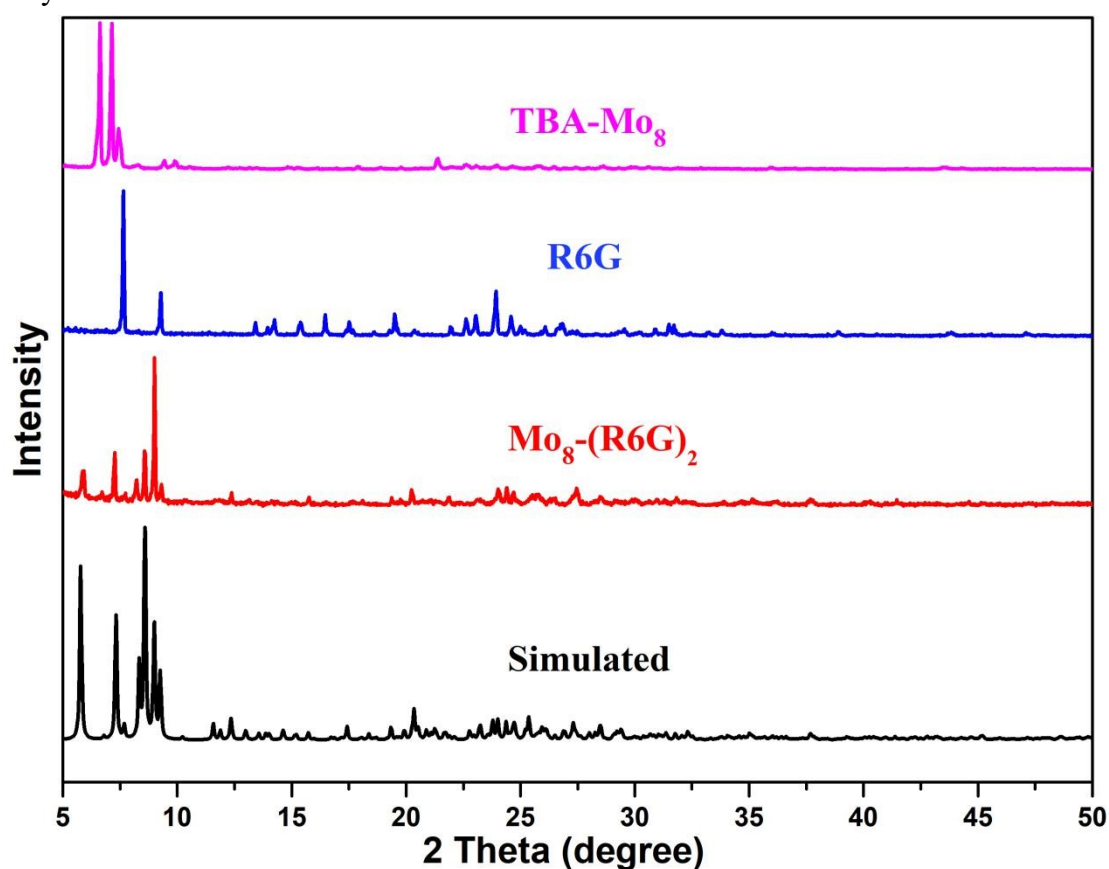


Fig. S7. Experimental (red, $\text{Mo}_8\text{-(R6G)}_2$; blue, R6G, TBA- Mo_8 , pink) and simulated (black) PXRD patterns.

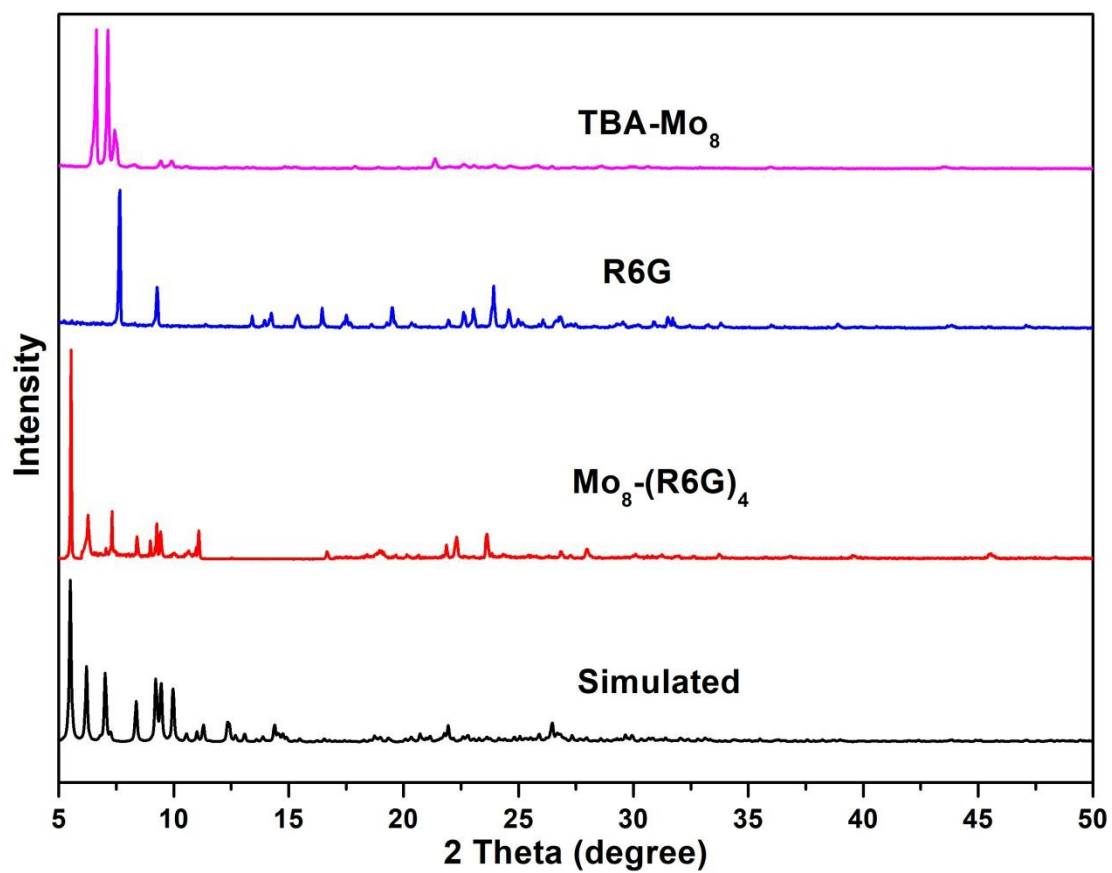


Fig. S8. Experimental (red, Mo₈-(R6G)₄; blue, R6G, TBA-Mo₈, pink) and simulated (black) PXRD patterns.

S7 Thermogravimetric analyses (TGA)

Fig. S9 shows that the thermal decomposition process of $\text{Mo}_8\text{-(R6G)}_2$, $\text{Mo}_8\text{-(R6G)}_4$, R6G and TBA- Mo_8 . $\text{Mo}_8\text{-(R6G)}_2$ display 25.1 % weight loss in the temperature range of 270-310 °C, corresponding to the removal of TBA and R6G molecule, while $\text{Mo}_8\text{-(R6G)}_4$ display 5.39 % weight loss in the temperature range of 290-310 °C, corresponding to the removal of R6G molecules. R6G display 9.72 % weight loss in the temperature range of 235-280 °C. TBA- Mo_8 display 33.72 % weight loss in the temperature range of 265-330 °C.

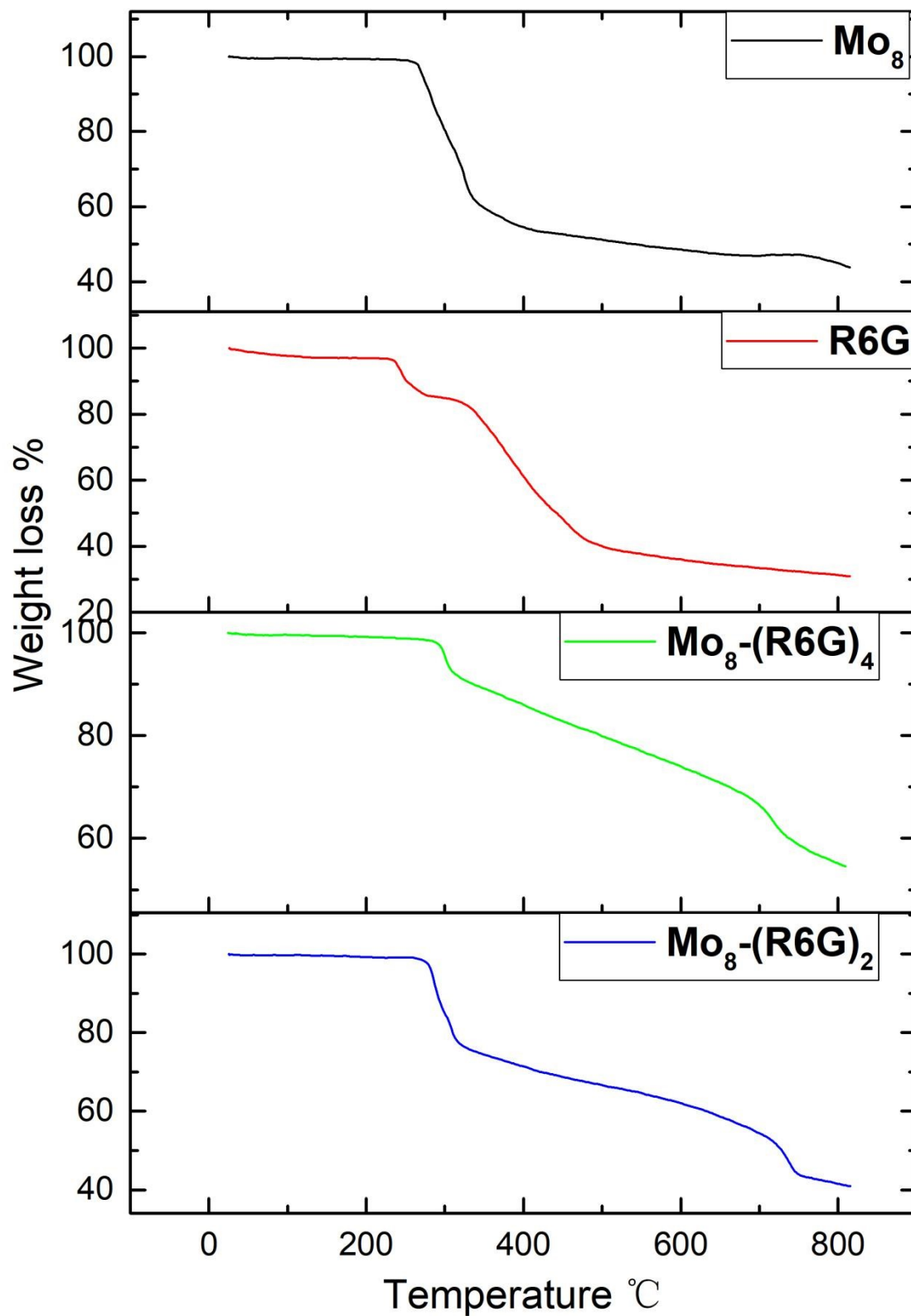


Fig. S9. The TGA curves of $\text{Mo}_8-(\text{R6G})_2$ (blue), $\text{Mo}_8-(\text{R6G})_4$ (green), R6G (red) and TBA- Mo_8 (black).

S8 UV-Vis absorption spectra

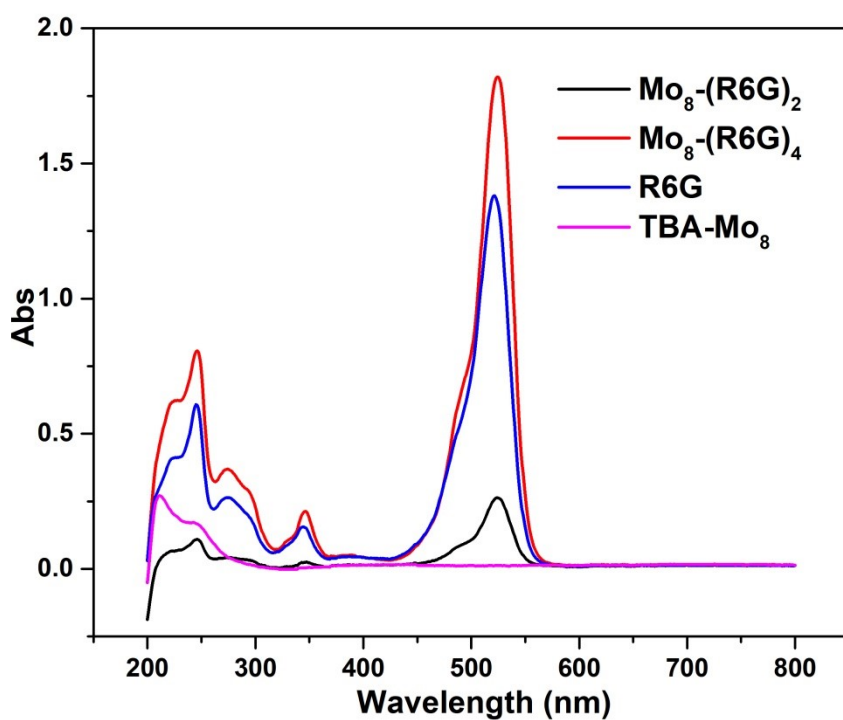


Fig. S10. The UV-vis absorption spectra of R6G (blue), TBA- Mo_8 (pink), $\text{Mo}_8\text{-(R6G)}_2$ (black) and $\text{Mo}_8\text{-(R6G)}_4$ (red) in CH_3CN at the concentration of a. c. 1×10^{-5} M.

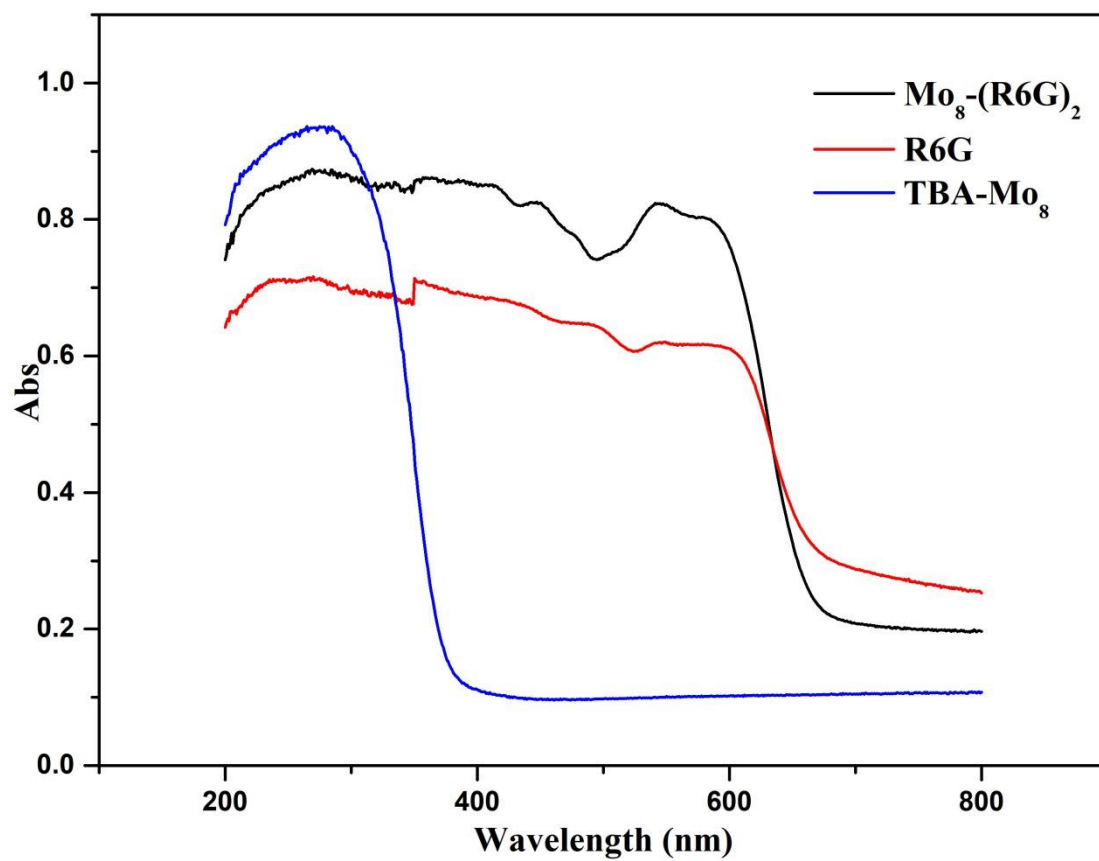


Fig. S11. The UV-vis diffuse reflectance spectra of R6G (red), TBA- Mo_8 (blue) and Mo_8 -(R6G)₂(black).

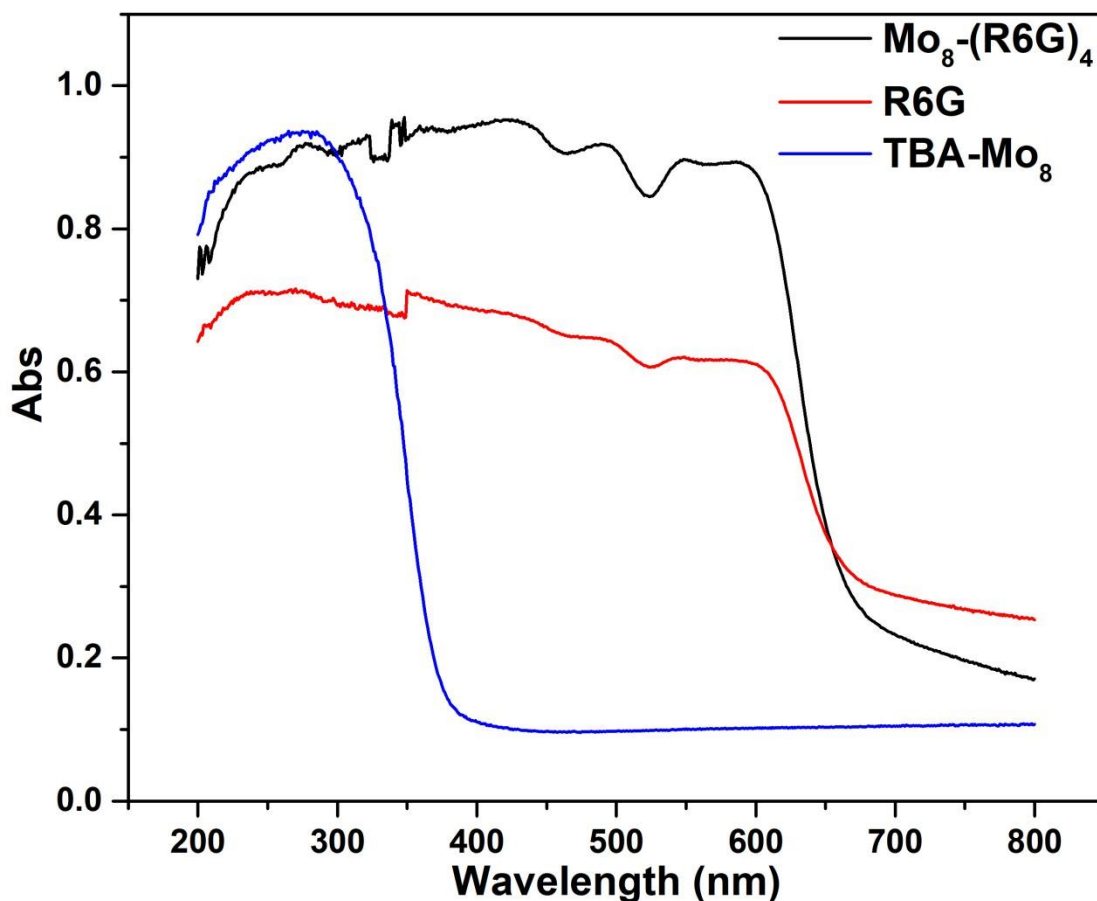
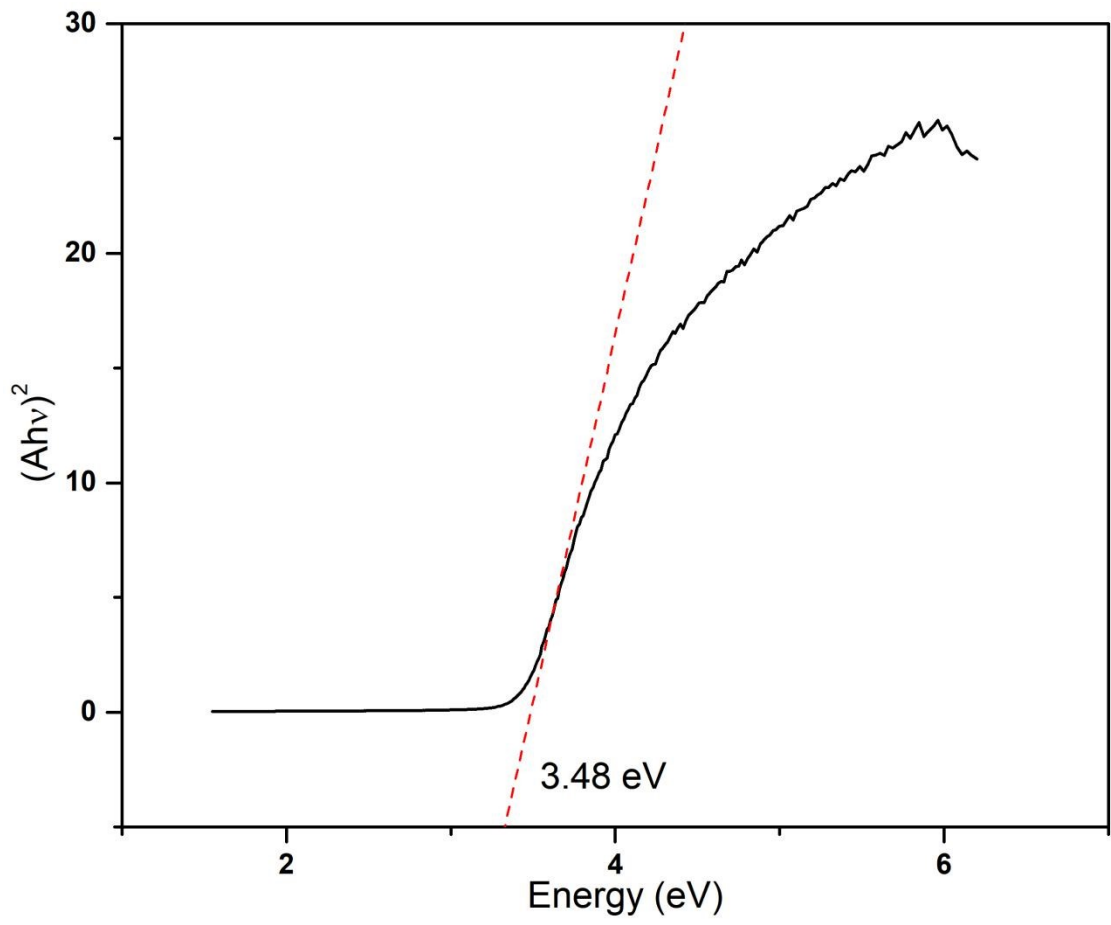


Fig. S12. The UV-vis diffuse reflectance spectra of R6G (red), TBA-Mo₈ (blue) and Mo₈-(R6G)₄ (black).

S9 The band gap

The band gap was measured by a solid-state UV-vis diffuse reflection at room temperature. According to the equation $(Ah\nu)^2 = K(h\nu - E_g)$ (A is the absorption, $h\nu$ is the discrete photo energy, K is a constant, E_g is the band gap energy), the extrapolated values (the straight lines to the x axis) of $h\nu$ at $A = 0$ give absorption edge energies. The E_g of Mo₈, R6G, Mo₈-(R6G)₂ and Mo₈-(R6G)₄ is 3.48 eV, 1.87 eV, 1.91 eV and 1.90 eV, respectively.



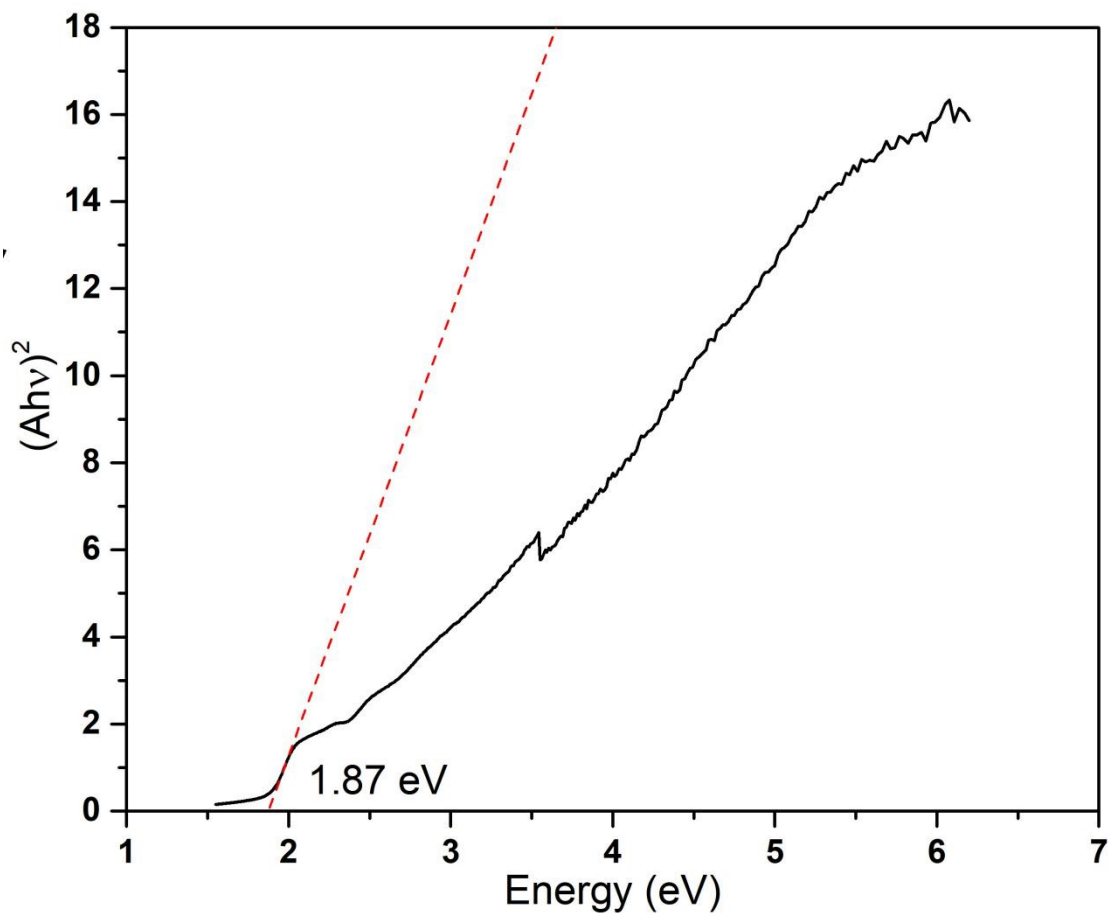


Fig. S13. The band gap of Mo₈ (up) and R6G (down).

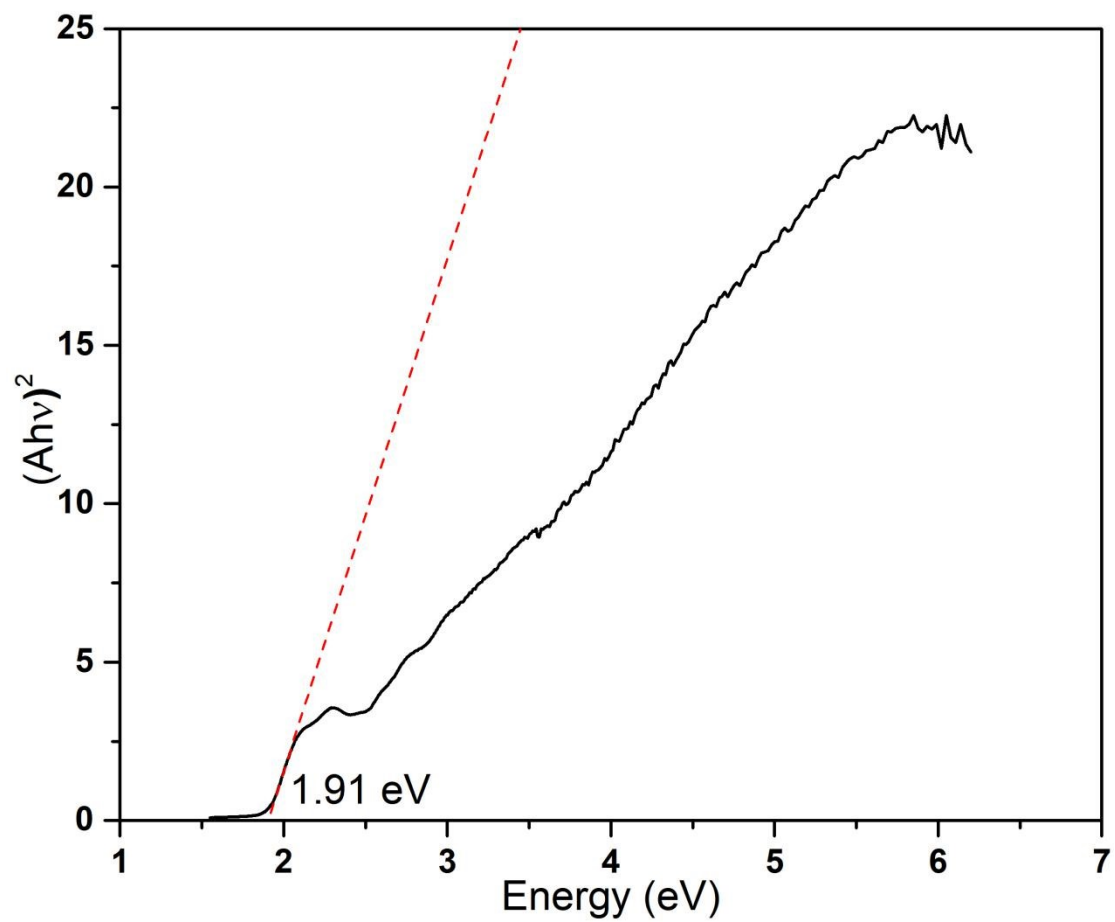


Fig. S14. The band gap of $\text{Mo}_8\text{-(R6G)}_2$.

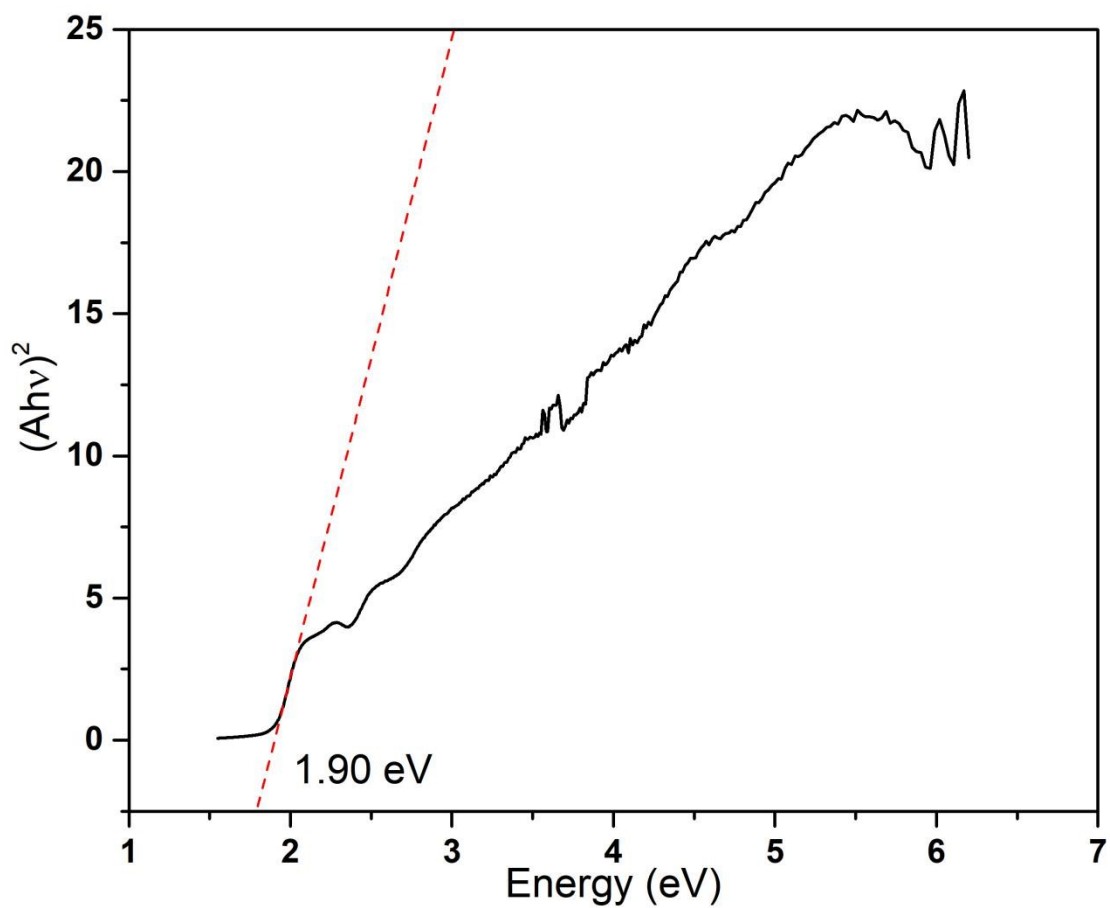


Fig. S15. The band gap of $\text{Mo}_8\text{-(R6G)}_4$.

S11 The Excitation spectroscopy of solid-state samples

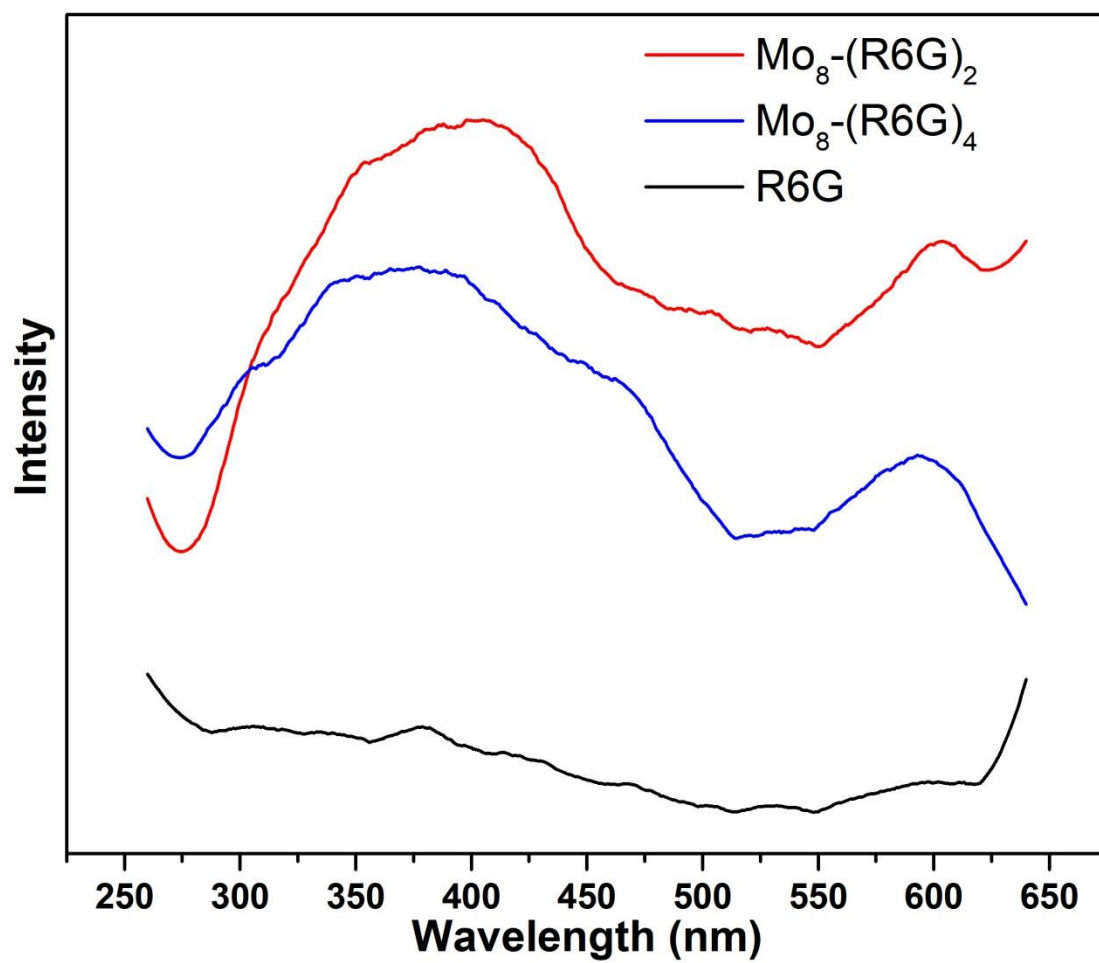


Fig. S16. The excitation spectrum of R6G(black), $\text{Mo}_8\text{-(R6G)}_2$ (red), $\text{Mo}_8\text{-(R6G)}_4$ (blue).

S11 The Steady state photoluminescence (PL) spectroscopy of solid-state samples

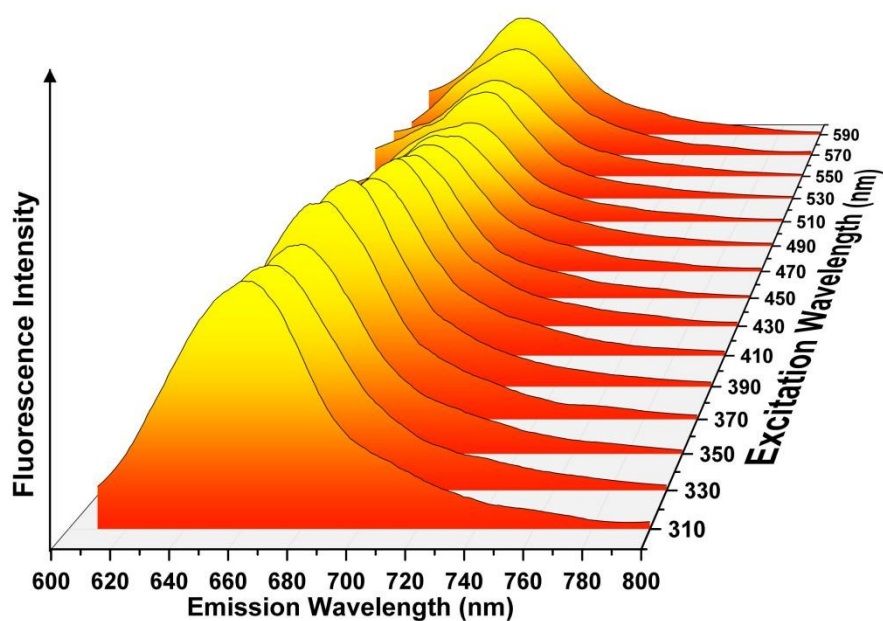


Fig. S20. The fluorescence emission spectra of R6G under different excitation wavelength.

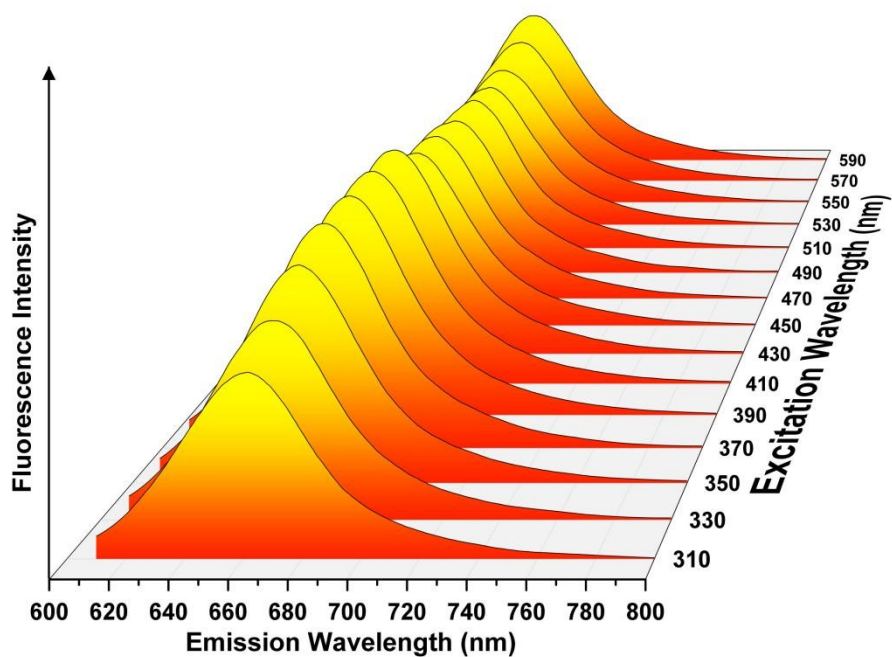


Fig. S21. The fluorescence emission spectra of Mo₈-(R6G)₂ under different excitation wavelength.

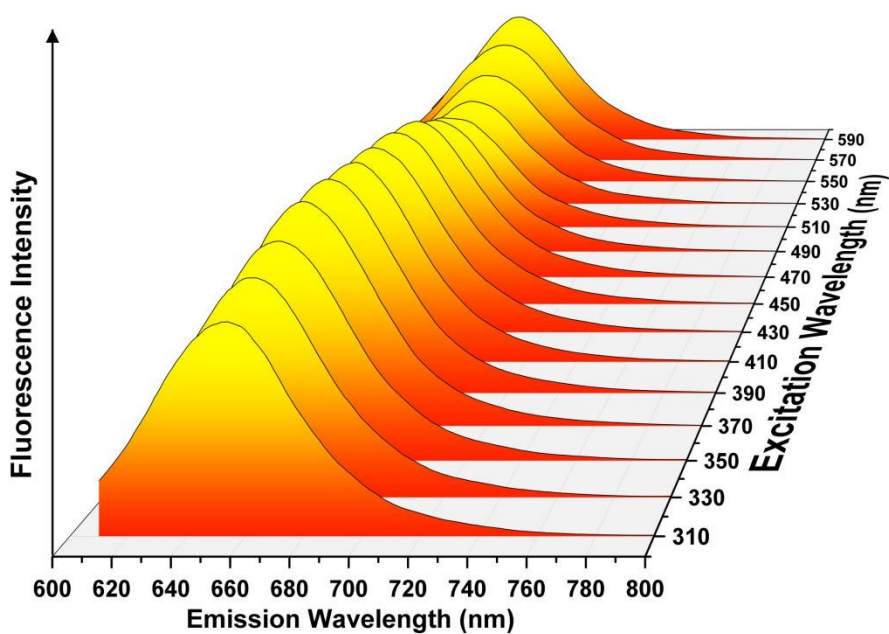


Fig. S22. The fluorescence emission spectra of Mo₈-(R6G)₄ under different excitation wavelength.

S12 Emission decay spectroscopy

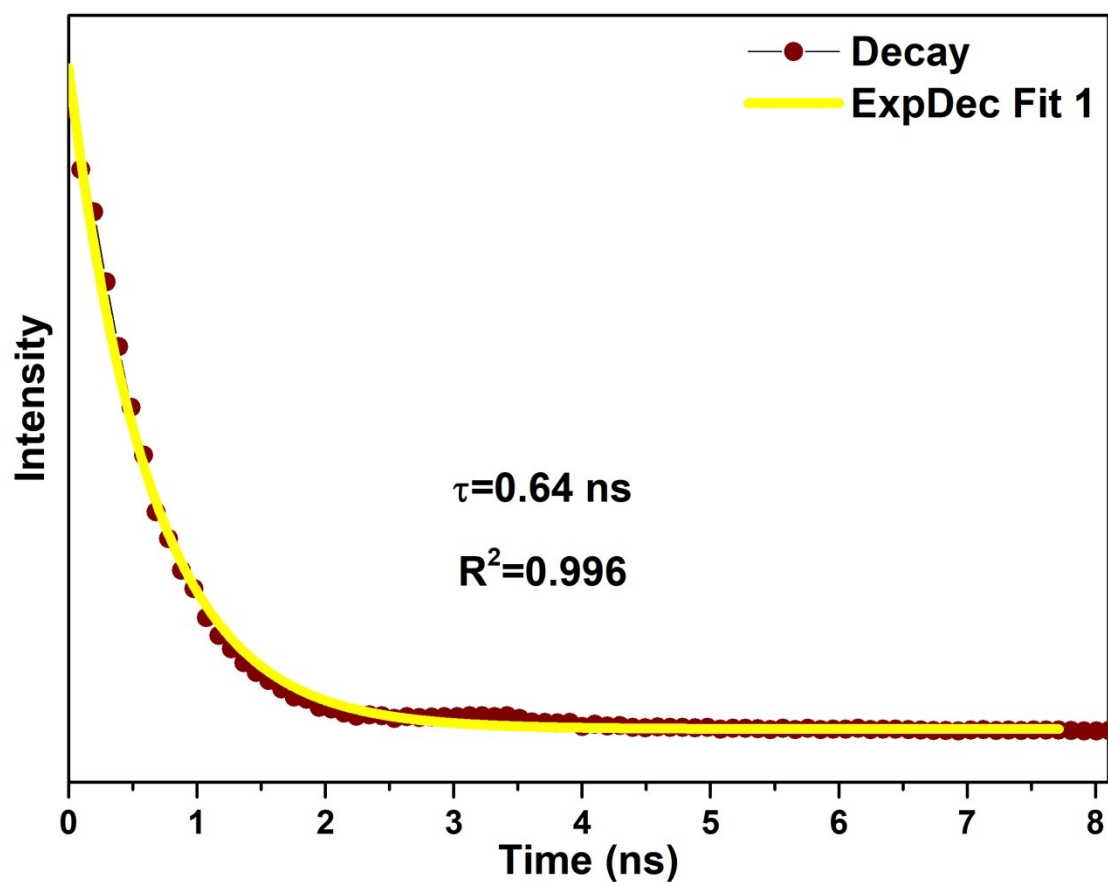


Fig. S23. Photoluminescence decay profile of R6G measured at 629 nm at 298 K using 330 NanoLed.

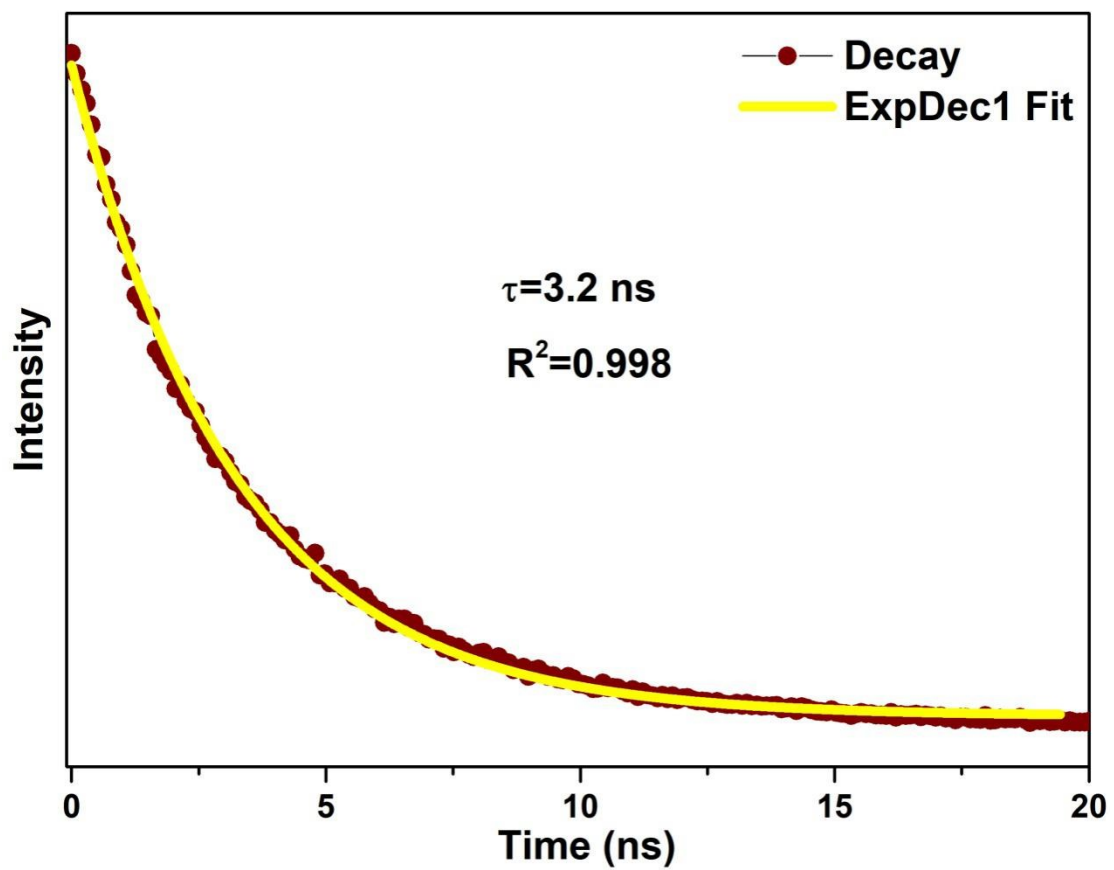


Fig. S24. Photoluminescence decay profile of $\text{Mo}_8\text{-(R6G)}_2$ measured at 629 nm at 298 K using 330 NanoLed.

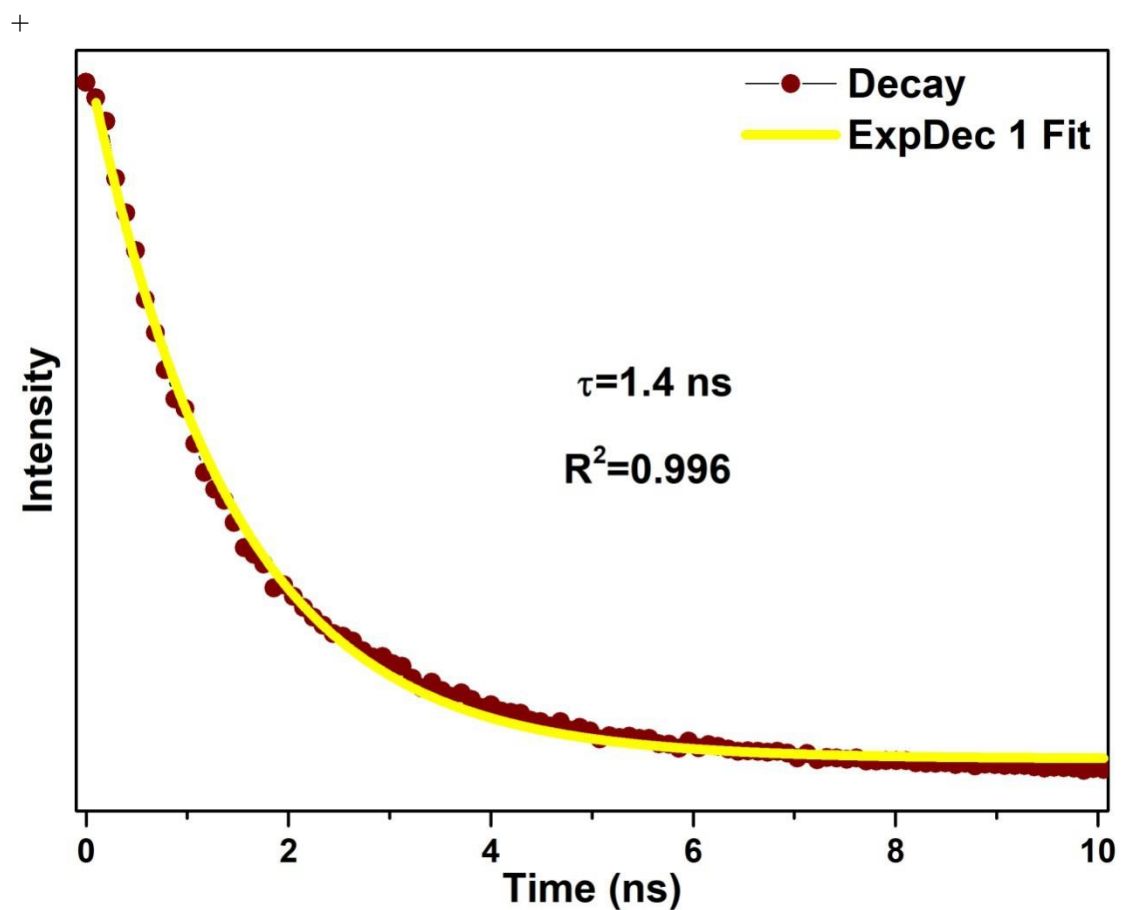


Fig. S25. Photoluminescence decay profile of $\text{Mo}_8\text{-(R6G)}_4$ measured at 629 nm at 298 K using 330 NanoLed.

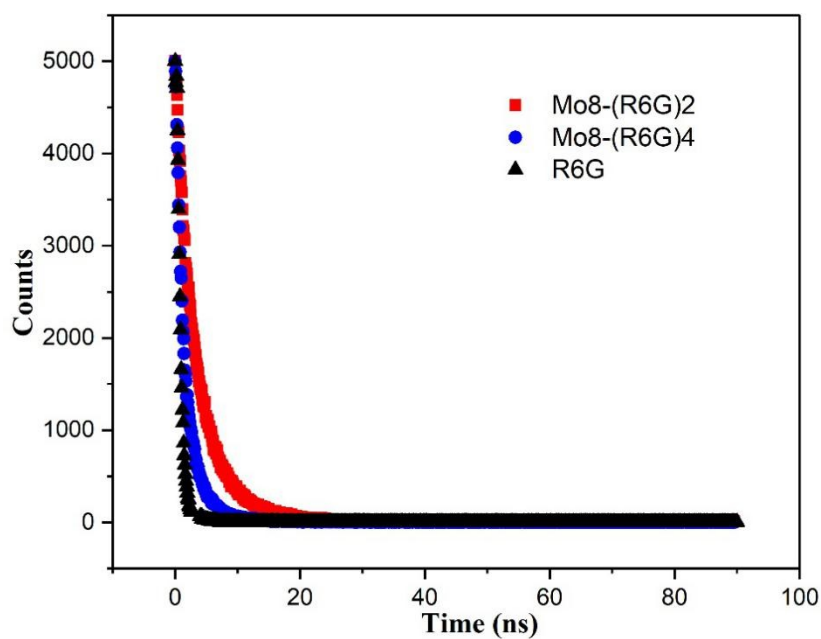


Fig. S26. Comparison of Photoluminescence decay profile of R6G, $\text{Mo}_8\text{-(R6G)}_2$ and $\text{Mo}_8\text{-(R6G)}_4$.

S13 The fluorescence emission spectra of CH₃CN solution

The luminescence of different ratios of [Mo₈O₂₆]⁴⁻ and R6G in CH₃CN is shown as Fig S27. The [Mo₈O₂₆]⁴⁻ quenches the luminescence of R6G in solution as the formation of ion pairs. The emission wavelength of R6G (emit red fluorescence) in solid state are around 660 nm, which is same as in the literature²⁻³. But it is red-shifted compared with the emission wavelength of R6G in the liquid (emit yellow fluorescence). This is due to the effect of the molecular plane (leading to π electron delocalization) and the interaction between molecules. The molecules in the solution are movable, but in the solid state are fixed, which limits the flexibility of the molecules and affects the distribution of electronic energy level.

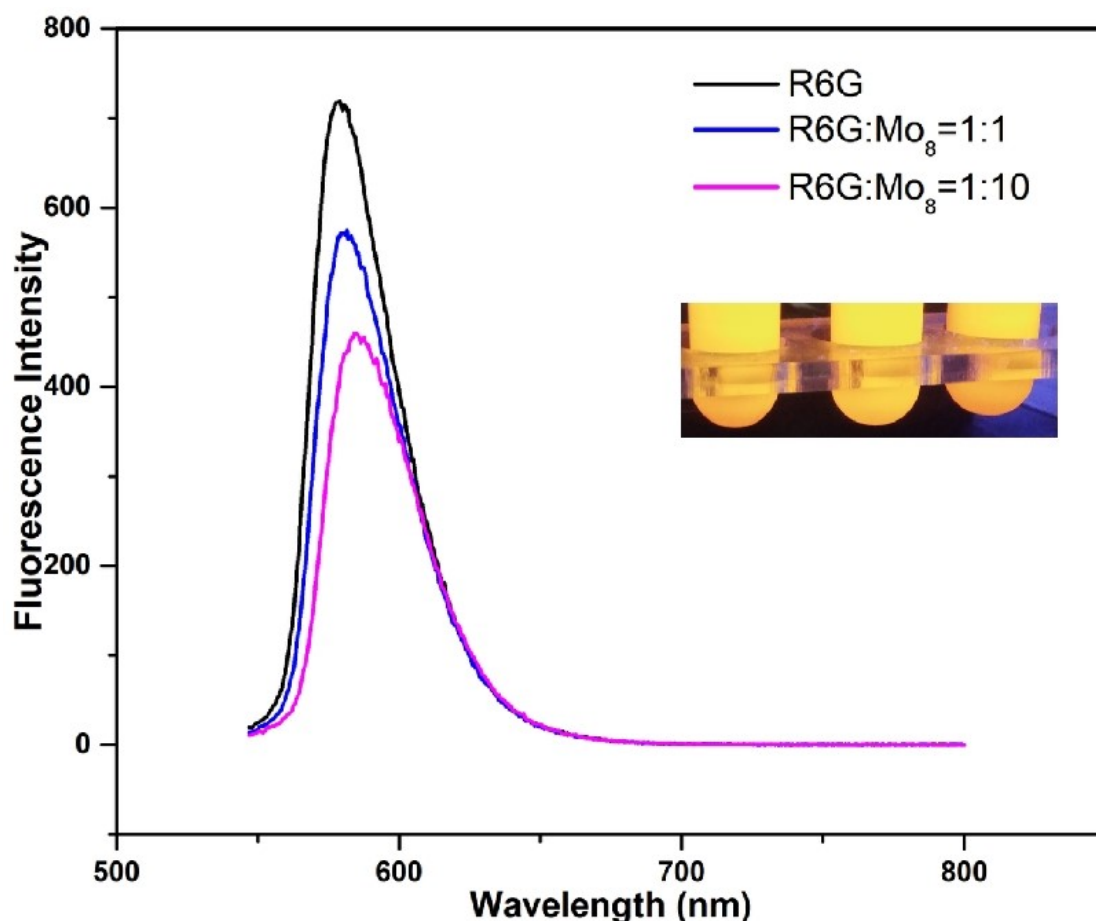


Fig. S27. The fluorescence emission spectra of R6G (black) and different ratios of Mo₈ added into R6G solution (2 mL, 0.01 g/mL).

The fluorescence emission spectra in CH₃CN solution was obtained on the F-2700 spectrometer with the maximum excitation wavelength of 527 nm (slit, 5 nm).

S14 Reference

- 1 Sheldrick, G. M. *Acta Cryst. A* **2008**, 64, 112.
2. Tripathi, S. K.; Monga, A.; Saini, G. S. S., Characterization of thermally evaporated thin films of Rhodamine 6G. *Smart Mater. Struct.* 2009, 18 (12), 125012-125018.
3. Han, T.-T.; Yang, J.; Liu, Y.-Y.; Ma, J.-F., Rhodamine 6G loaded zeolitic imidazolate framework-8 (ZIF-8) nanocomposites for highly selective luminescent sensing of Fe³⁺, Cr⁶⁺ and aniline. *Micropor. Mesopor. Mat.* 2016, 228, 275-288.